Medical Imaging 2012: Physics of Medical Imaging,
Proc. of SPIE Vol. 8313, doi: 10.1117/12.910584

Sound field directivity in multi-element synthetic transmit aperture method for ultrasound imaging

Y. Tasinkevych[*a], Z. Klimonda[a], M. Lewandowski[a], I. Trots[a], A. Nowicki[a]
[a]Institute of Fundamental Technological Research of the Polish Academy of Sciences,
5b Pawinskiego str., Warsaw, 02-106, Poland;

ABSTRACT

A modified multi-element synthetic transmit aperture (MSTA) method for ultrasound imaging with RF echoes correction taking into account the influence of the element directivity is presented. The property is significant as the element width becomes commensurable with the wavelength of the emitted signal. The angular dependence of the radiation efficiency of the transmit/receive aperture is obtained from exact solution of the corresponding mixed boundary-value problem for periodic baffle system, modeling the transducer array. It is evaluated at the nominal frequency of the excitation signal and is implemented in the developed MSTA algorithm as apodization weights calculated for each imaging point and all combinations of the transmit/receive apertures. The performance of developed method is tested using FIELDII simulated synthetic aperture data of the point reflectors to estimate the visualization depth and lateral resolution. Besides, a FIELDII simulated and measurement data of cyst phantom are used for qualitative assessment of the imaging contrast. Comparison of the results obtained by the modified and conventional MSTA algorithms is given which reveals considerable improvement of the image quality in the area neighboring to the transducer's aperture, and increase of the visualization depth at the cost of slight degradation of lateral resolution near the transducer face.

Keywords: synthetic aperture, ultrasound imaging, beamforming

1. INTRODUCTION

The synthetic aperture methods (SA) are well known and widely deployed in radar techniques. Increasing processing power of modern computers allows effective implementation of SA technique in medical ultrasound systems with multi-element probes. Several methods were proposed to form a synthetic aperture in ultrasound imaging. Among them a multi-element synthetic transmit aperture (MSTA) technique[1,2], which uses a several elements in transmitting and all elements in receiving, is the one providing the full dynamic focusing in both transmit and receive modes, thus giving the imaging quality comparable to the conventional phased arrays. The common approach to the SA in medical ultrasound assumes the single element of multi-element probe as a point source transmitting the spherical wave-front. This simplification is reasonable for the element size much smaller than the wavelength of transmitted waveform. However, the element size of modern probes is often comparable to the wavelength of the emitted signal. Hence, its directivity influences the generated sound field and proper correction of RF echoes in SA method could improve the quality of the final image. To solve this problem the modified multi-element synthetic aperture method is presented which takes into account the transmit/receive element directivity for the case when its lateral width is comparable with the wavelength corresponding to the operating frequency. For this purpose a system of predefined apodization weights is introduced into the scheme of the back-scattered RF echoes coherent summation for each focus point in the image and all possible combinations of the transmit/receive pairs. The weights are evaluated for each image point by means of the directivity functions of the transmit/receive apertures, obtained from the exact solution of a mixed boundary-value problem for periodic baffle system, modeling the transducer array[3]. Aperture apodization techniques are widely used in the ultrasonic imaging systems for modification and controlling of the beam pattern[4]. Different approaches are presented in the literature. In the simplest case a pre-defined fixed weights corresponding to typical window functions are applied to recorded RF signals from different channels during dynamical focusing of the received beam[5]. To obtain more flexible control over transmitted and received wave-fields, the optimal sets of weights generated for each focus point in the image are applied

[*] yurijtas@ippt.gov.pl; phone (48-22) 8261281; fax (48-22) 8269815

in order to synthesize specified beam patterns[6] or to obtain specific lateral field distribution at each, user controlled, depth[7]. Recently great attention in SA ultrasound imaging is drawn by the adaptive beamformin[8]. The apodization weights are data-dependent and are dynamically updated for each point in the synthesized image. Typically, adaptive beamforming techniques are characterized by intense computational loading (inversion of large ill-conditioned matrices for each imaging point, for example) and are not suitable for real-time synthetic aperture applications.

As shown in the following in this paper the application of proposed apodization weights considerably improves the penetration depth and diminishes the hazy blurring artefacts observable in the case of the regular MSTA algorithm, particularly in the imaging region near the transducer aperture at the cost of slight decrease in the lateral resolution in this area.

The paper is organized in the following way. In the next section the brief discussion of the MSTA algorithm is given. In Sec. 3 the modified algorithm is introduced and discussed in details. In Sec. 4 a brief discussion concerning the mixed boundary-value problem for periodic baffle system modeling the transducer array is given. In Sec. 5 numerical examples which present performance of the proposed modified MSTA algorithm are shown for 4 MHz 128-element transducer array with 0.3 mm pitch and 0.02 mm kerf using synthetic aperture data for point reflectors simulated by FIELDII[9,10] and measurement data for cyst phantom (Dansk Fantom Service, model 571) collected using the SonixTOUCH Research system (Ultrasonix Medical Corporation, Richmond, BC, Canada). The scanner was equipped with a linear transducer model L14-5/38: a 128-element transducer with 0.3 mm element pitch, 0.02 mm kerf and 70% fractional bandwidth was excited by 3 cycles of transducer's center frequency equal 4 MHz. Finally, in Section 6 the conclusion of this work are summarized.

2. MULTI-ELEMENT SYNTHETIC TRANSMIT APERTURE METHOD

In the MSTA approach at each emission a multiple-element transmit aperture is used as it is illustrated in Fig. 1.

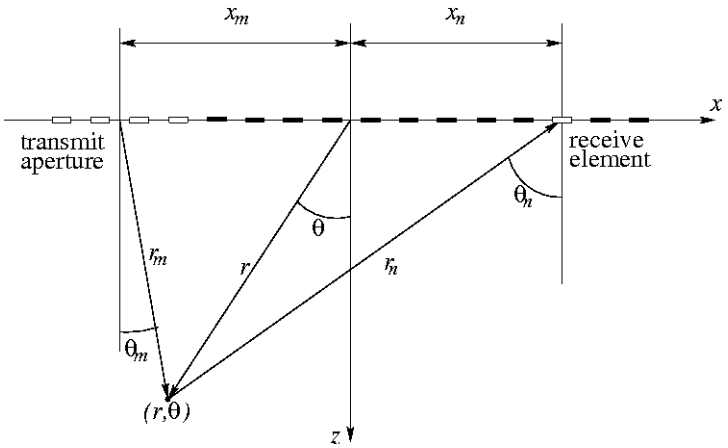

Figure 1. Transmit and receive elements combination and the focal point in MSTA method.

The back-scattered waves are received by each element independently and the resulting RF echo signals are digitized and stored for further processing. For an N-element array, N_t-element transmit aperture and N_{sh}-element shift of the transmit aperture between subsequent emissions, there are $M=\lceil (N-N_t)/N_{sh} \rceil$ emissions in each cycle altogether, where $\lceil x \rceil$ is the integer ceiling of x. Assuming $N_t=1$ results in conventional STA algorithm. In the case of MSTA the frame rate is increased by N/M as compared to the STA method due to decrease of the total number of emissions, which speeds up the data acquisition process. Thus, for N-element aperture upon completion of the data acquisition cycle $M\times N$ RF echo signals are recorded for further image synthetisation. To this end the coherent summation of all received RF echoes is performed. For the N-element array for each point in the image, the final focused signal can be expressed as follows:

$$A_{MSTA}(r,\theta)=\sum_{m=1}^{M}\sum_{n=1}^{N} y_{m,n}\left(\frac{2r}{c}-\tau_{m,n}\right), \quad (1)$$

where $y_{m,n}(t)$ is the RF echo signal and $\tau_{m,n}$ is the round-trip delay defined for the (m, n) transmit/receive combination by expression:

$$\tau_{m,n} = \tau_m + \tau_n, \quad 1 \le n \le N, \quad 1 \le m \le M. \tag{2}$$

The corresponding delays for m^{th} transmit and n^{th} receive elements relative to the imaging point (r,θ) are:

$$\tau_i = \frac{1}{c}\left(r - \sqrt{r^2 + x_i^2 - 2x_i r \sin\theta}\right), \quad i = m,n, \tag{3}$$

where x_m, x_n are the positions of the m^{th} transmit and n^{th} receive elements, respectively, and r, θ are the polar coordinates of the imaging point with respect to the origin, placed in the center of the transducer's aperture. The first and the second summations correspond to the transmit and receive focusing, respectively. It should be noted that the angular dependence is not taken into account in the applied point-like source model. However, when the width of the array element is comparable to the wavelength, corresponding to the nominal frequency of the emitted signal, the point-like source model becomes inaccurate. The directivities of the individual transmit and receive elements influence the partial contributions of the resulting signal $A(r,\theta)$ in Eq. (3) depending on the mutual positions of the imaging point and transmit/receive pair, determined by the angles θ_m, θ_n (see Fig. 1). The next section highlights the differences between the above and the developed modified MSTA algorithms.

3. MODIFIED MULTI-ELEMENT SYNTHETIC TRANSMIT APERTURE METHOD

In this section a modified MSTA imaging algorithm which accounts for the element directivity function and its influence on the total signal $A(r,\theta)$ is presented. The underlying idea can be illustrated referring to the following example. Assume the case when two similar reflectors are located at the points with polar coordinates (r_i,θ_i); i=1, 2, and consider the m^{th} element of the transducer array acting as transmitter as depicted in Fig. 2. For simplicity a single-element transmit aperture is considered without loss of generality. The corresponding RF echo signal received by the same element is $y_{m,m}(t)$. As r_{1m}=r_{2m}, both reflectors contribute to the corresponding echo signal $y_{m,m}(t)$ simultaneously due to the equal round-trip propagation time $2r_{im}/c$; i=1, 2. Obviously, the scattering amplitude of the reflector #1 located at the point (r_1, θ_1) is dominant, since the angle θ_{1m} coincides with m^{th} element's normal direction (direction of its maximum radiation), whereas its transmit-receive efficiency at the angle θ_{2m}, corresponding to the reflector #2, is lower. If the focus point coincides with location of the reflector #2, the partial contribution from $y_{m,m}(t)$ to $A(r_2,\theta_2)$ evaluated from Eq. (3) in addition to the signal scattered from the reflector #2 (being relatively small due to the large observation angle θ_{2m}), introduces the spurious echo from the reflector #1. Since it is placed in the normal direction with respect to the considered m^{th} element, the corresponding false contribution is expected to be large, which eventually results in an excessive increase of the signal amplitude at the point (r_2,θ_2) of the final image.

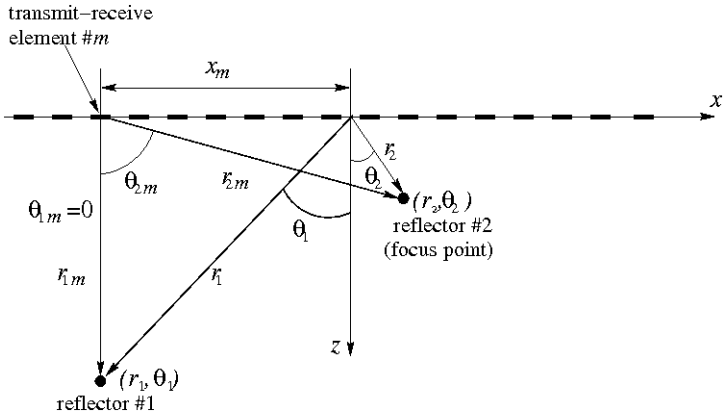

Figure 2. Influence of the reflector #1 located at the point (r_1, θ_1) on the value of resulting signal $A(r_2, \theta_2)$ for focus point (r_2, θ_2), coinciding with location of reflector #2.

To overcome this difficulty, a proper spatial filtering, accounting for the observation angle in accordance with the transmit/receive element directivity function, is needed. Assume that the angular directivity function of the considered element is known and denoted by $f(\theta_m)$, where θ_m is measured from the m^{th} element normal direction (see Fig. 2). To suppress the influence from the reflector #1 on the value of the imaging signal $A(r_2,\theta_2)$ at the focus point (r_2,θ_2), coinciding with location of the reflector #2, the partial contribution of the echo $y_{m,m}(t)$ is weighted by the corresponding value of $f(\theta_{2m})$. This corresponds to the spatial filtering of the superposed signal in accordance with the positions of the focus point and transmit-receive elements, accounting for their angular directivity functions. The above considerations lead to the following modification of the MSTA imaging algorithm using arbitrary number of elements in transmit mode:

$$A_{MSTA}^{\mathrm{mod}}(r,\theta)=\sum_{m=1}^{M}\sum_{n=1}^{N} w_{mn}\, y_{m,n}\left(\frac{2r}{c}-\tau_{m,n}\right),$$
$$w_{mn}=f_T(\theta_m)\, f_R(\theta_n),\ \theta_i=\theta_i(r,\theta),\ i=m,n, \tag{4}$$

where $\theta_i(r,\theta)$, $i=m,n$ are the corresponding observation angles for the transmit/receive elements and $f_T(\theta_m)$, $f_R(\theta_n)$ are their directivity functions, respectively. Note, that the angles θ_m and θ_n depend on the spatial position of the focus point (r,θ). In the case of STA algorithm[11] the corresponding directivity function of single-element transmit and receive apertures, which is used for evaluation of weights w_{mn}, can be calculated in the far-field approximation using analytical expression[12]:

$$f(\theta)=\frac{\sin(\pi d/\lambda\sin\theta)}{\pi d/\lambda\sin\theta}\cos\theta, \tag{5}$$

where d is the element width, and λ is the wavelength. The above Eq. (5) applies to a strip transducer with a time harmonic uniform pressure distribution along its width and is obtained by means of the Rayleigh-Sommerfeld formula in the far-field region[13]. In the case of MSTA method discussed here, the analytic formula given in Eq. (5) cannot be used for evaluation of the directivity function of the multi-element transmit aperture (although it could be applied to compute the weights for the single-element receive aperture). Here, instead, the results of the solution of a mixed boundary-value problem for periodic baffle array[3] will be used in order to evaluate the corresponding directivity functions. The next section highlights the main results of the full-wave analysis[3] which are relevant to the proposed modified MSTA algorithm.

4. DIRECTIVITY FUNCTION OF THE MULTI-ELEMENT APERTURE

In this section a brief discussion on the solution of a mixed boundary-value problem for periodic baffle system modeling the transducer array[3] is given. Namely, this approach allows to evaluate the directivity functions of the transmit/receive apertures needed for apodization weights calculation in Eq. (4). The solution of the corresponding boundary-value problem is sought in spatial spectrum domain (k-space). Namely, the spatial spectrum (Fourier transform) of the pressure distribution on a baffle plane is of main concern and is used for the far-field radiation pattern evaluation. The method allows to take into account the mutual interactions of the array elements in the full-wave analysis of the wave excitation or scattering problems in contrast to the model of a single strip transducer[13], Eq. (5), used in the case modified STA algorithm[12]. In the considered mixed boundary-value problem the normal acoustic vibration vanishes on baffles[14] (strips) and between them there are acoustically soft domains where the acoustic pressure vanishes, or is given constant values in the case of the wave excitation problem. The solution is obtained using a so called BIS-expansion method[15] which was successfully used earlier for solving electrostatic problems in the theory of surface acoustic waves interdigital transducers[16], in the theory of elastic wave scattering by periodic cracks[17], and in generalized form in the theory of electromagnetic wave scattering by periodic gratings[18]. The directivity function of the periodic system of hard acoustic baffles (periodicity along the x-axis direction is assumed, see Fig. 1) can be evaluated from the spatial spectrum of the pressure field distribution on the baffle plane as follows[3]:

$$f(\theta)\sim p(k\sin\theta)\cos\theta;\quad k=\frac{\omega}{c}=\frac{2\pi}{\lambda}, \tag{6}$$

where k - is the wave-number; c - is the sound velocity; ω - is the angular temporal frequency; p - is the spatial spectrum of the pressure distribution on the plane of baffles, which is the solution of the above boundary-value problem and can be written as follows[3]:

$$p(\xi) = p_n(\xi - nK) \equiv p_n(r); \quad \xi = r + nK; \quad n = \lfloor \xi \rfloor, \quad K = 2\pi / \Lambda, \tag{7}$$

where ξ - is the spatial spectrum variable related to x spatial coordinate; $\lfloor \xi \rfloor$ - is the integer floor of ξ; $r \in (0,K)$ is an arbitrary spatial wave-number constrained to one Brillouin zone for the sake of uniqueness of the pressure distribution representation on the plane z=0:

$$p(x) = \sum_n p_n \mathrm{e}^{-j(r+nK)x}, \quad p_n = \frac{j}{r+nK} \sum_m \alpha_m S_{n-m} P_{n-m}(\cos\Delta); \quad \Delta = \pi(1 - d/\Lambda), \tag{8}$$

where p_n - are the Bloch amplitudes; P_n - are the Legendre polynomials; d - is the baffle width and Λ is the system period (transducer pitch); S_n=1 for $n \geq 0$ and 0 otherwise. In Eq. (8) α_m are unknown expansion coefficients (dependent on r) representing the corresponding Bloch components p_n. The α_m are computed from the system of linear equations[3]:

$$\begin{aligned} &\sum_m \alpha_m \left[j\frac{\eta}{\xi} S_{n-m} - 1 \right] P_{n-m}(\cos\Delta) = 0, \\ &\sum_m (-1)^m \alpha_m P_{-r/K-m}(-\cos\Delta) = j\frac{K}{\pi} \tilde{p}_l e^{jrl\Lambda} \sin \pi r / K, \end{aligned} \tag{9}$$

where $\tilde{p}_l = 1$, l=0,…, N_{tr-1} and 0 otherwise are given constant pressures of the corresponding active elements (slots in the considered boundary-value problem formulation) which model the N_{tr}-element transmit aperture. In Eq. (9) the summation over a finite domain $m \in [-M, M+1]$ is assumed and $n \in [-M, M]$, or in the other words, there are $2M$+1 Bloch orders accounted for in the expansion for $p(x)$, Eq. (8). The truncation index M is determined by the BIS-expansion approximation stating that for $m > M$ the assumption $\eta/\xi = jS_\xi$ holds (see the cited work for more details), where η is the spatial spectrum variable related to the z spatial coordinate and is defined as follows:

$$\eta = \sqrt{k^2 - \xi^2} = -j\sqrt{\xi^2 - k^2}, \tag{10}$$

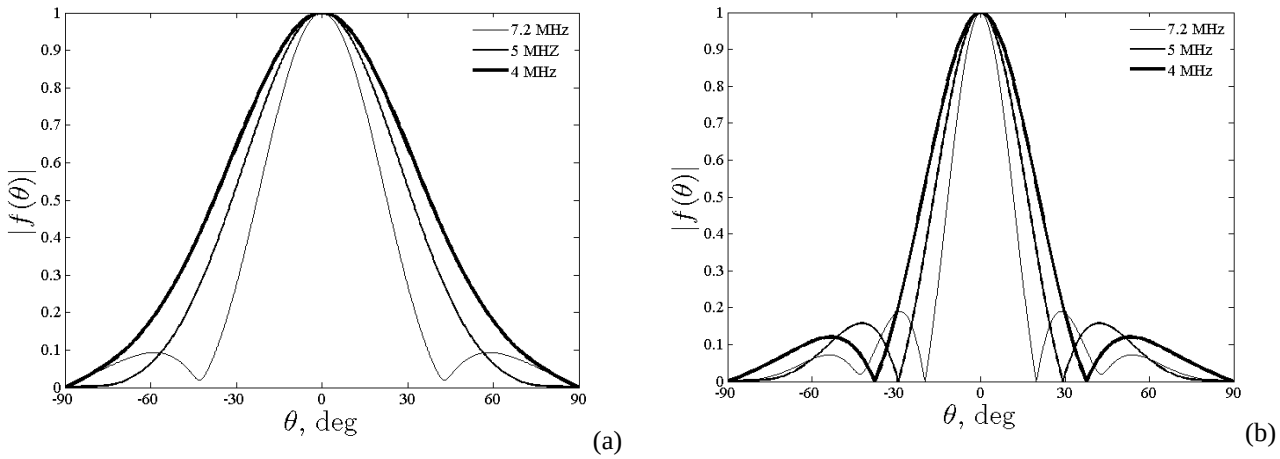

Figure 3. Directivity functions (a) N_{tr}=1 and (b) N_{tr}=2 for different frequencies of excitation signal: 4, 5, 7.2 MHz corresponding to d/λ=0.75, 0.94, 1.35;element width d=0.28 mm and 0.02 mm kerf is assumed.

In the above equation the value of η is chosen in order to satisfy the radiation condition of the acoustic field at $z \to \infty$. Typically, for $k \sim K$ it is sufficient to take into account only several Bloch components p_n in the solution for the pressure field in Eq. (8) (in the numerical examples shown below M=16 is applied). In the case of a single-element receive

aperture to evaluate its directivity function and corresponding apodization weights (see Eq. (4)) instead of Eq. (5) the above method, Eq. (6), is used with $\tilde{p}_l = \delta_{l0}$ applied in Eq. (9), where δ- is the Kronecker delta.

Some computed examples of the directivity function evaluated for different values of the ratio d/λ and λ/Λ and N_{tr}=1 along with N_{tr}=2 are shown in Fig. 3. The values of d/λ and operating frequencies in Fig. 3 correspond to the ones which are used in the numerical examples shown in the next section. The directivity function given by Eq. (6) is used in the modified MSTA algorithm, Eq. (4), for apodization weights evaluation, both in the case transmit ($f_T(\theta)$) and receive ($f_R(\theta)$) apertures.

5. NUMERICAL RESULTS AND DISCUSSION

In this section the proposed modified MSTA algorithm is tested using the data obtained by FIELDII[9,10] program for Matlab® and from experimental measurements. To verify the performance of the modified MSTA algorithm and estimate the lateral resolution and penetration depth as compared to the conventional MSTA, the FIELDII simulated synthetic aperture data of point reflectors were used. The case of 4 MHz 128-element transducer array with the 0.3 mm pitch and 0.02 mm kerf was considered. The point reflectors were placed in 7 columns, each spaced 4.9 mm apart laterally (this corresponds to 16 transducer pitches). The columns were centered with respect to the transducer middle point for convenience. In each column reflectors were spaced 5 mm axially. Such arrangement of point reflectors, covering entire imaging region, was considered to be convenient for visual assessment of the imaging quality in the whole area. The resulting 2D visualization of point reflectors is shown in Fig. 4 over a 60 dB dynamic range.

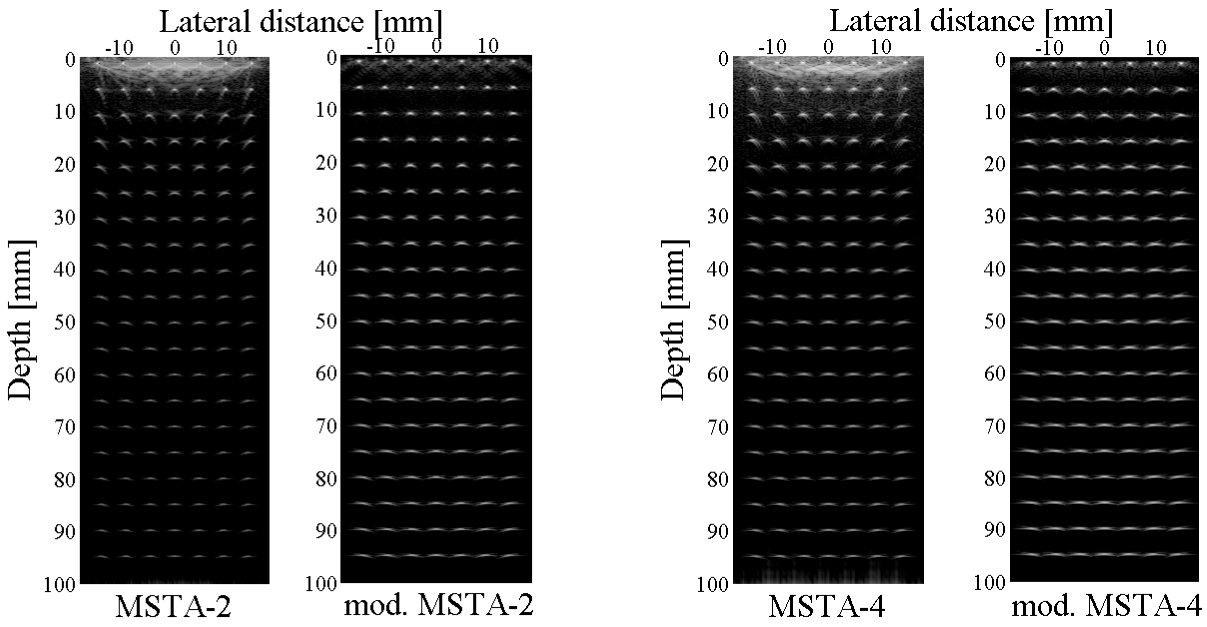

Figure 4. Comparison of the image reconstruction by the conventional (left subplot) and modified (right subplot) MSTA algorithms of the FIELD II simulated synthetic aperture data for point reflectors and 4 MHz 128-element transducer array with 0.3 mm pitch and 0.02 mm kerf; (a) N_{tr}=2, (b) N_{tr}=4. All images are displayed over 60 dB dynamic range

Considerable improvement of the image quality in the region adjacent to the transducer's aperture can be observed. The blurring artefacts clearly visible in the case of the conventional MSTA algorithm (left subplots in Figs. 4(a), 4(b)) in the vicinity of the first row of point reflectors, are substantially reduced in the case of the modified MSTA algorithm (right subplots). This is clearly observable in Figs. 5, 6 where the lateral cross-section of the first row of point reflectors and the axial section of the central column are shown, respectively (only 4 first reflectors are visualized for convenience).

As seen in Figs. 5 and 6, the "noise"-like spatial variations of the scattered signal from the reflectors positioned near the transducer surface are substantially suppressed from approximately −20 dB (MSTA, N_{tr}=2) to −37 dB (modified MSTA, N_{tr}=2), see Fig. 5(a), and from −25 dB (MSTA, N_{tr}=4) to −35 dB (modified MSTA, N_{tr}=4), see Fig. 5(b). Also, an increase in penetration depth can be observed in Fig. 6 which is further illustrated in Fig. 7, where a detailed view of the axial section (central column) showing the maxima of the scattered echo signals as a function of depth is presented. As shown in Figs. 7(a), 7(b) for N_{tr}=2, the scattered echo amplitude obtained using the modified MSTA algorithm is 3.67 and 3.74 times larger than that obtained by means of the conventional one at the depths of 50 and 90 mm, respectively. Similarly, from Figs. 7(c), 7(d) for N_{tr}=4 it is seen that the scattered echo amplitude increases by 1.52 and 1.75 at the same depths if the modified algorithm is used.

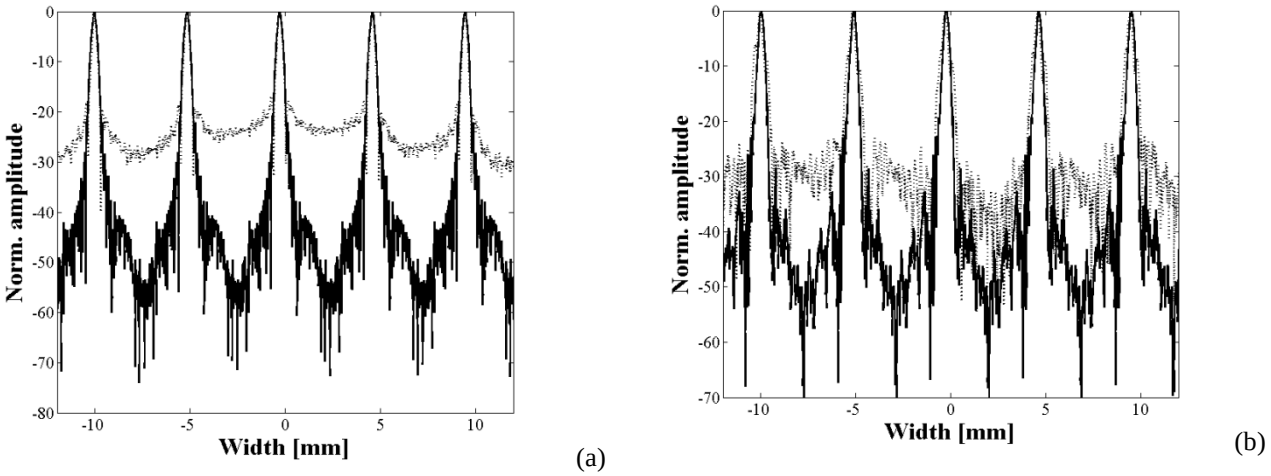

Figure 5. Lateral cross-section of the first row (depth 1 mm) of point reflectors in logarithmic scale; (a) N_{tr}=2, (b) N_{tr}=4; solid lines - modified MSTA algorithm, this work; dotted lines - regular MSTA algorithm.

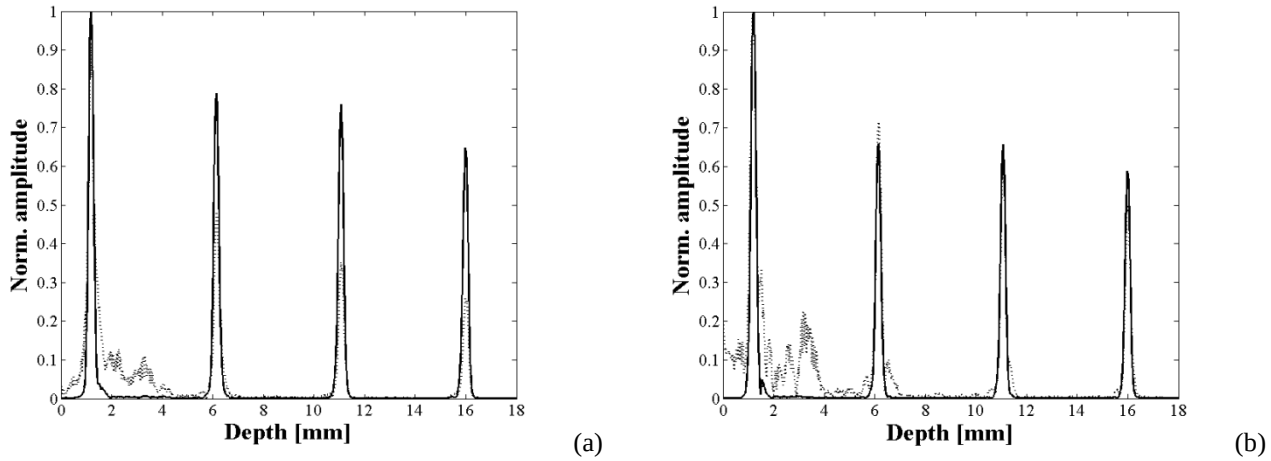

Figure 6. Axial section of the central column of point reflectors: a) N_{tr}=2, b) N_{tr}=4; solid lines - modified MSTA algorithm, this work; dotted lines - regular MSTA algorithm.

In Fig. 8 the results related to the lateral resolution are summarized. The lateral cross-sections corresponding to the scattered echo signals of the point reflectors positioned in the central column at the depths of 50 and 90 mm

are shown. The cases of N_{tr}=2 and N_{tr}=4 are considered. As shown in Figs. 8(a) through 8(d) for modified MSTA algorithm the lateral resolution is slightly decreased as compared to the conventional one. It is quantified here by the full width at half maximum (FWHM). Accordingly, at the axial distance of 50 and 90 mm for the conventional MSTA the lateral resolution is 0.88 and 1.06 mm in the case of N_{tr}=2. For N_{tr}=4 the corresponding data are 0.93 and 1.12. In the case of the modified MSTA algorithm at the depths of 50 and 90 mm the lateral resolution is 0.91 and 1.07 mm if the 2-element transmit aperture is used (N_{tr}=2). For N_{tr}=4 the corresponding data are 1.01 and 1.16 mm. These represent 4.16 and 1.21% for N_{tr}=2 along with 8.08 and 3.16 % for N_{tr}=4 decrease in the lateral resolution at the above identified depths. It is worth noting that the decrease in the lateral resolution diminishes with depth.

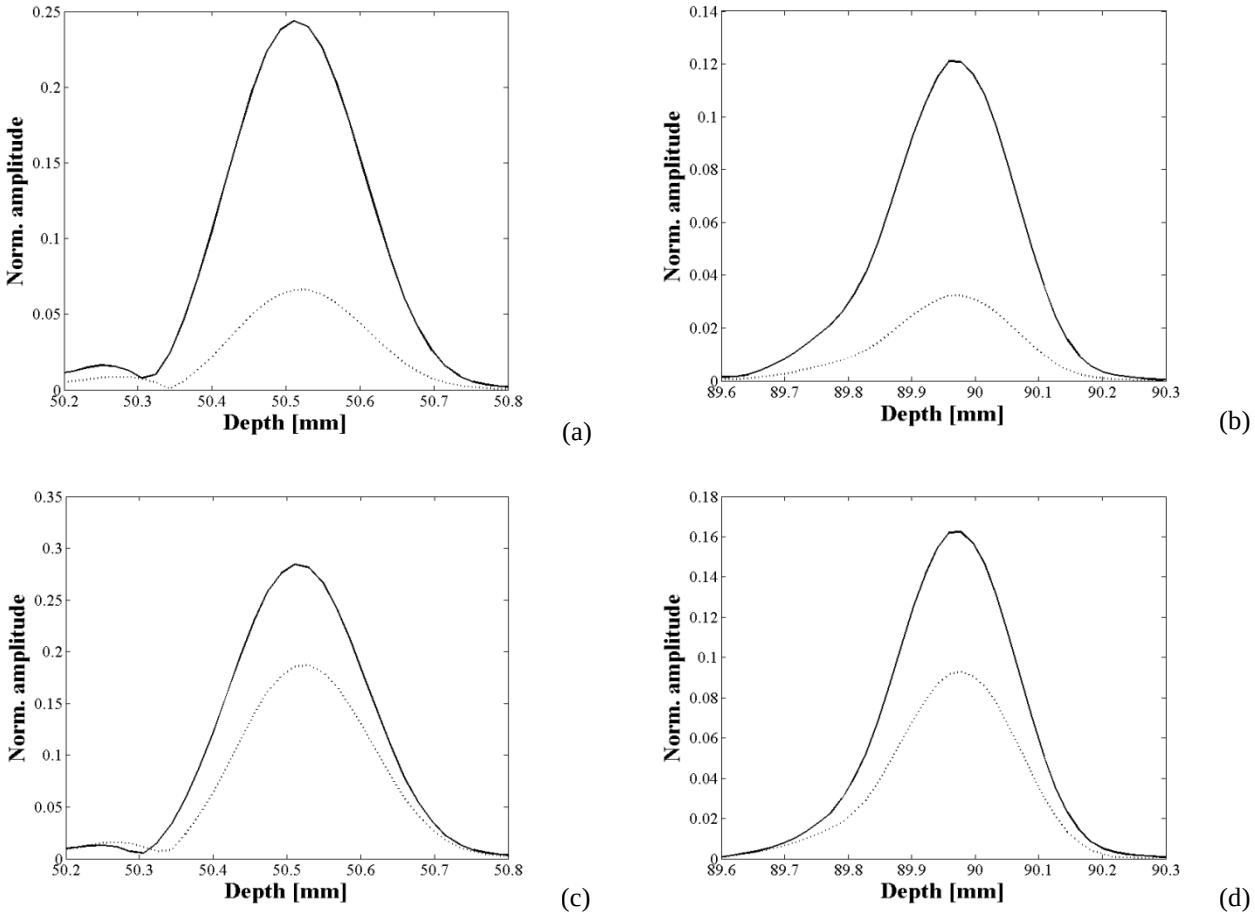

Figure 7. Normalized axial section of the image line coinciding with the central column of point reflectors at different depths: (a) 50 mm, N_{tr}=2; (b) 90 mm, N_{tr}=2; (c) 50 mm, N_{tr}=4; (d) 90 mm, N_{tr}=4. Thick solid lines – modified MSTA algorithm, this work; dotted lines – conventional MSTA algorithm.

In Fig. 9 the improvements in the image contrast offered by the modified MSTA algorithm are demonstrated. For this purpose the performance of the modified MSTA algorithm was tested using the experimentally obtained synthetic aperture data of a cyst phantom (an extra large scan- and elevation-plane tissue mimicking phantom model 571[19] Dansk Fantom Service). The measurements were done using the Sonix-TOUCH Research system (Ultrasonix Medical Corporation). The scanner was equipped with a linear transducer model L14-5/38: a 128-element transducer with 0.3 mm element pitch, 0.02 mm kerf and 70% fractional bandwidth was excited by 3 cycles of transducer's center frequency equal 4 MHz. As anticipated (see Section 3), the images presented in Fig. 9 show that the modified MSTA algorithm provides a considerable improvement of the image quality in the immediate vicinity of the array's aperture (see Fig. 2 and Fig. 5), as compared to the conventional MSTA. Also, the results shown in Fig. 9, demonstrate that the image

contrast of the cysts located at the axial distance exceeding 40 mm is also slightly improved (visual assessment). In Fig. 9(c) the modified MSTA algorithm is compared both with the conventional one and with the MSTA, having the apodization weights applied only in receiving[20], since for the transmit apertures comprised of more than 8-10 elements the directivity becomes too intensive. From Fig. 9(c) it is seen that for larger transmit apertures the corresponding apodization can be applied in the receive mode only, which still yields considerable improvement of the imaging quality as compared to the conventional MSTA algorithm, see Fig.9(c).

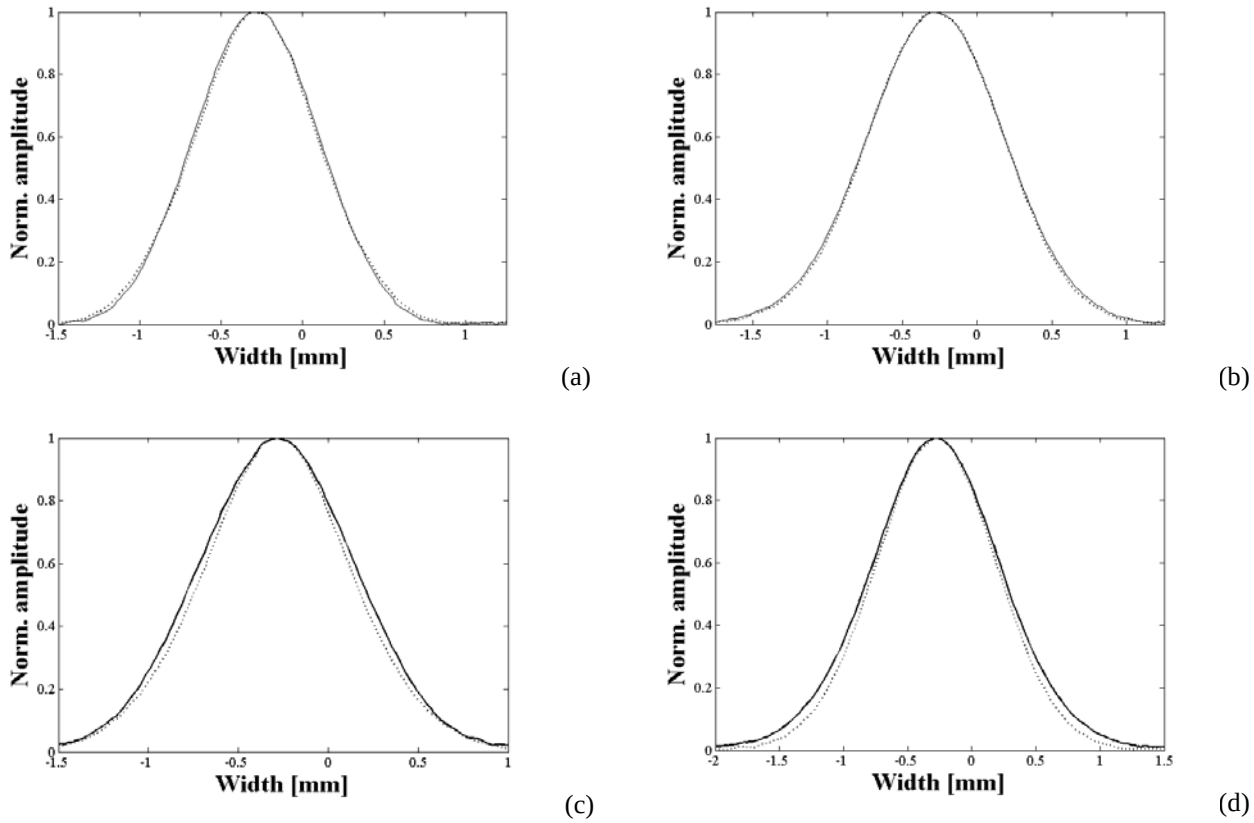

Figure 8. Normalized lateral cross-section of the scattered signal corresponding to the point reflectors placed in central column at different depths: (a) 50 mm, N_{tr}=2; (b) 90 mm, N_{tr}=2; (c) 50 mm, N_{tr}=4; (d) 90 mm, N_{tr}=4. Thick solid lines – modified MSTA algorithm, this work; dotted lines – conventional MSTA algorithm.

6. CONCLUSIONS

In this work the modified multi-element synthetic transmit aperture (MSTA) algorithm for ultrasound imaging was presented and discussed. The modification is based on weighted summing of the properly delayed RF echoes. The corresponding weights are evaluated using angular directivity functions of the corresponding transmit/receive elements for each focus point in the image. For efficient computation of the far-field radiation patterns the results of the previous study concerning the analysis of generation and scattering of the acoustic waves by periodic baffle system were used. The predicted improvements in the image quality and the penetration depth were verified using measured synthetic aperture data of cyst phantom and FIELDII[9,10] simulated synthetic aperture data of point reflectors. It was shown, that using the modified MSTA a considerable improvement in the image quality in the “near field” region lying in the immediate vicinity of the transducer surface was observed. Also, the hazy blurring artefacts observable in the images obtained using the conventional synthetic aperture algorithm were substantially suppressed due to the directivity weights applied in the modified MSTA. In addition, an increase in the penetration depth was demonstrated. Concurrently, however, a slight degradation of the lateral resolution was observed. On the other hand this decrease in the lateral resolution diminishes with increasing penetration depth.

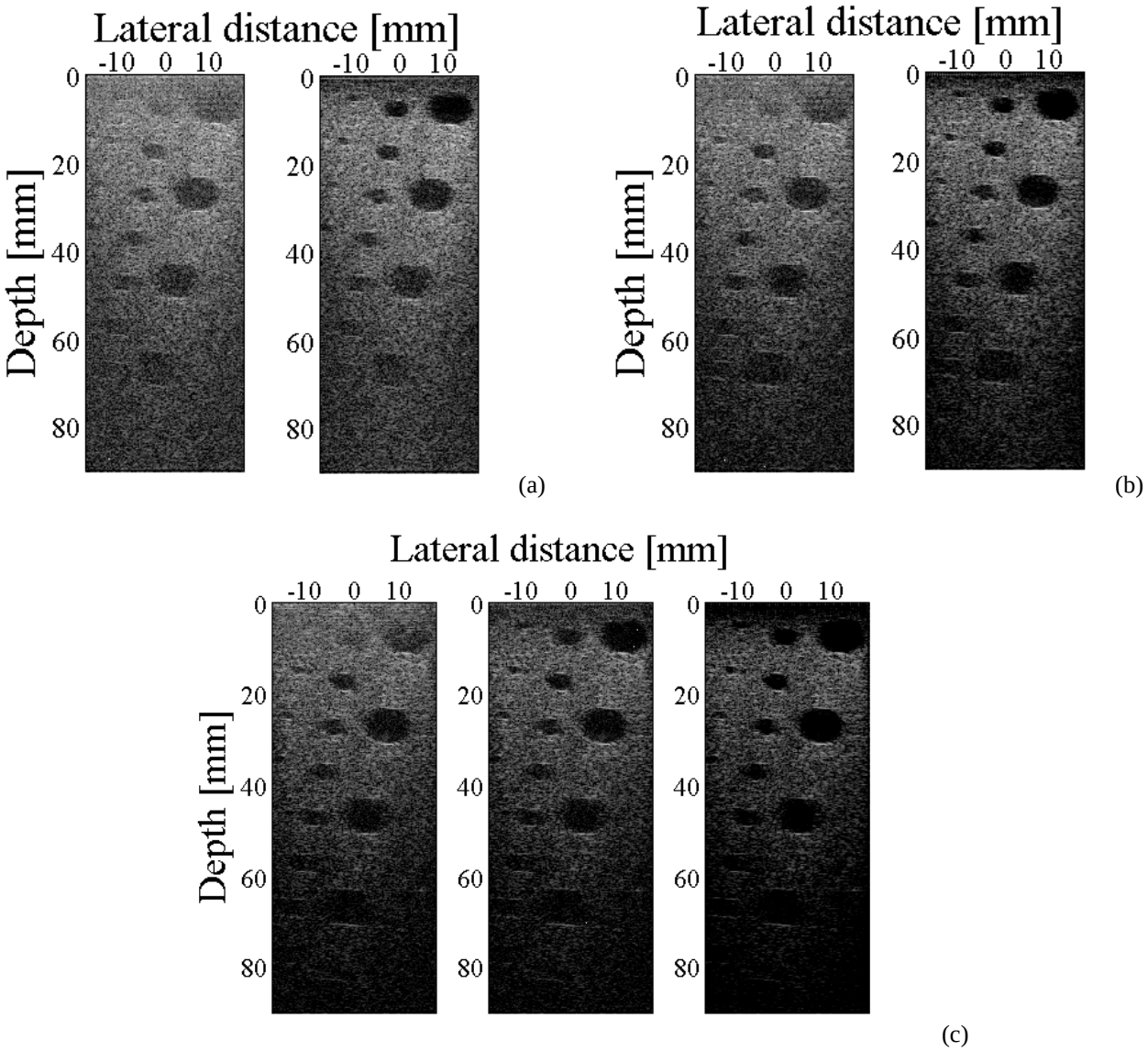

Figure 9. Image reconstruction of the measurement synthetic aperture data for cyst phantom (Dansk Fantom Service, model 571[19]) and 4 MHz 128-element transducer array with 0.3 mm pitch and 0.02 mm kerf a) N_{tr}=2, b) N_{tr}=4, c) N_{tr}=8. All images are displayed over 40 dB dynamic range. Left subplot – conventional MSTA algorithm; right subplot – modified MSTA algorithm, this work; (c) central subplot – modified MSTA algorithm with apodization weights applied in receive mode only.

It was demonstrated that the proposed algorithm can be applied to improve the visualization quality in both transmit and receive modes for transmit aperture comprised of up to 8-10 elements. For larger apertures the increased angular directivity of the transmit aperture leads to stronger spatial filtering in wider range of angles. But, as it was demonstrated, in such cases the proposed apodization weights can be applied in receive mode only, which still yields considerable improvement of the imaging quality as compared to the conventional MSTA algorithm. This limitation is not, however, a dramatic drawback of the proposed modified MSTA method. Usually, in the MSTA method applications not large number of elements in transmit mode is used[21], since there exists a trade-off between the penetration depth and the lateral resolution: the former increases and the latter does the opposite as the number of elements in transmit aperture increases[22].

ACKNOWLEDGMENT

Project POIG.01.03.01-14-012/08-00 co-financed by the European Regional Development Fund under the Innovative Economy Operational Programme. Project is governed by Ministry of Science and Higher Education, Poland.

REFERENCES

[1] Holm, S., Focused multi-element synthetic aperture imaging, Department of Informatics, University of Oslo, (1995).
[2] Gammelmark, K., L., Jensen, J., A., "Multielement synthetic transmit aperture imaging using temporal encoding," IEEE Trans. Med. Imag. 22 (4), 552–563, (2003).
[3] Tasinkevych, Y., Danicki, E., J., "Wave generation and scattering by periodic baffle system in application to beam-forming analysis, "Wave Motion 48 (2), 130–145, (2011).
[4] P. J. Thoen, P., J., "Aperture apodization to reduce the off-axis intensity of the pulsed-mode directivity function of linear arrays," Ultrasonics 20 (5), 231–236, (1982).
[5] Wright, J., N., Hanafy, A., "Resolution issues in medical ultrasound, " IEEE Trans. Ultrason., Ferroelect., Freq. Cont. 33 (1), 91–91, (1986).
[6] Repetto, S., Trucco, A., "A stochastic approach for the apodization of very short arrays, " Ultrasonics 42, 425–429, (2004).
[7] Sakhaei, S., M., Mahloojifar, A., Ghassemian, H., "A transformation based method to design ultrasound array, " Ultrasonics 49 (2), 179–184, (2009).
[8] Nikolov, S., I., Jensen, J., A., Tomov, B., G., "Fast parametric beamformer for synthetic aperture imaging," IEEE Trans. Ultrason., Ferro elect., Freq. Cont. 55 (8), 1755–1767, (2008).
[9] Jensen, J., A., Svendsen, N., B., "Calculation of pressure fields from arbitrarily shaped, apodized, and excited ultrasound transducers, "IEEE Trans. Ultrason., Ferroelect., Freq. Cont. 39 (2), 262–267, (1992)
[10] Jensen, J., A., " Field: A program for simulating ultrasound systems, " Proc. 10th Nordic-Baltic Conference on Biomedical Imaging published in Medical & Biological Engineering & Computing 34 (1), 351–353, (1996).
[11] Tasinkevych, Y., Trots, I., Nowicki, A., Lewin, P., A., "Modified synthetic transmit aperture algorithm for ultrasound imaging," Ultrasonics (2011), doi:10.1016/j.ultras.2011.09.003.
[12] Selfridge, A., R., Kino, G., S., Khuriyakub, B., T., "A theory for the radiation pattern of a narrow-strip acoustic transducer," Appl. Phys. Lett. 37 (1), 35–36, (1980).
[13] Goodman, J., W., Introduction to Fourier Optics, McGraw-Hill, Roberts and Company Publishers, (2005).
[14] Erbas, B., "Scattering of sound waves by an infinite grating composed of rigid plates, " Wave Motion 44, 282-303, (2007).
[15] Bløtekjær, K., Ingebrigtsen, K., A., Skeie, H., A., "A method for analyzing waves in structures consisting of metal strips on dispersive media," IEEE Trans. Electron. Device 20, 1133-1138, (1973).
[16] Danicki, E., J., Tasinkevych, Y., "Nonstandard electrostatic problem for strips, " J. Electrostat., 64 (6), 386-391, (2006).
[17] Danicki, E., J., "Scattering by periodic cracks and theory of comb transducers," Wave Motion 35, 355-370, (2002).
[18] Tasinkevych, Y., "Electromagnetic Scattering by Periodic Grating of Pec Bars, " J Electromagn. Waves Appl., 25 (5-6), 641-650, (2011).
[19] http://fantom.dk/571.htm
[20] Trots, I., Nowicki, A., Lewandowski, M., Tasinkevych, Y., "Multi-element synthetic transmit aperture in medical ultrasound imaging", Arch. Acoust. 35 (4), 687–699, (2010).
[21] Karaman, M., Pai-Chi Li, O'Donnell, M., " Synthetic aperture imaging for small scale systems, " IEEE Trans. Ultrason., Ferroelect., Freq. Cont. 42 (3), 429-442, (1995).
[22] Tasinkevych, Y., Trots, I., Nowicki, A., "Optimization in the multi-element synthetic transmit aperture method for ultrasound imaging, " Proc. 31th Conference “Acoustical Imaging”, Warsaw, Apr. 2011 (in press).